In vivo nanoparticle imaging of innate immune cells can serve as a marker of disease severity in a model of multiple sclerosis

Klara Kirschbaum[a,b,1], Jana K. Sonner[a,1], Matthias W. Zeller[c,d], Katrin Deumelandt[a], Julia Bode[e,f], Rakesh Sharma[e,f], Thomas Krüwel[e,f], Manuel Fischer[b], Angelika Hoffmann[b], Milene Costa da Silva[g,h,i], Martina U. Muckenthaler[g,h], Wolfgang Wick[j,k], Björn Tews[e,f], John W. Chen[c,d], Sabine Heiland[b], Martin Bendszus[b], Michael Platten[a,j], and Michael O. Breckwoldt[a,b,2]

[a]German Cancer Consortium, Clinical Cooperation Unit Neuroimmunology and Brain Tumor Immunology, German Cancer Research Center (DKFZ), 69120 Heidelberg, Germany; [b]Department of Neuroradiology, University Hospital Heidelberg, 69120 Heidelberg, Germany; [c]Center for Systems Biology, Massachusetts General Hospital, Harvard Medical School, Boston, MA 02115; [d]Division of Neuroradiology, Department of Radiology, Massachusetts General Hospital, Harvard Medical School, Boston, MA 02115; [e]Schaller Research Group, University of Heidelberg and DKFZ, 69120 Heidelberg, Germany; [f]Molecular Mechanisms of Tumor Invasion, DKFZ, 69120 Heidelberg, Germany; [g]Department of Pediatric Hematology, Oncology and Immunology, University of Heidelberg, 69120 Heidelberg, Germany; [h]Molecular Medicine Partnership Unit, University Hospital Heidelberg, 69120 Heidelberg, Germany; [i]Graduate Program in Areas of Basic and Applied Biology, Abel Salazar Biomedical Sciences Institute, University of Porto, 4050-313 Porto, Portugal; [j]Department of Neurology and National Center for Tumor Diseases (NCT), University Hospital Heidelberg, 69120 Heidelberg, Germany; and [k]German Cancer Consortium, Clinical Cooperation Unit Neurooncology, DKFZ, 69120 Heidelberg, Germany

Innate immune cells play a key role in the pathogenesis of multiple sclerosis and experimental autoimmune encephalomyelitis (EAE). Current clinical imaging is restricted to visualizing secondary effects of inflammation, such as gliosis and blood–brain barrier disruption. Advanced molecular imaging, such as iron oxide nanoparticle imaging, can allow direct imaging of cellular and molecular activity, but the exact cell types that phagocytose nanoparticles in vivo and how phagocytic activity relates to disease severity is not well understood. In this study we used MRI to map inflammatory infiltrates using high-field MRI and fluorescently labeled cross-linked iron oxide nanoparticles for cell tracking. We confirmed nanoparticle uptake and MR detectability ex vivo. Using in vivo MRI, we identified extensive nanoparticle signal in the cerebellar white matter and circumscribed cortical gray matter lesions that developed during the disease course (4.6-fold increase of nanoparticle accumulation in EAE compared with healthy controls, $P < 0.001$). Nanoparticles showed good cellular specificity for innate immune cells in vivo, labeling activated microglia, infiltrating macrophages, and neutrophils, whereas there was only sparse uptake by adaptive immune cells. Importantly, nanoparticle signal correlated better with clinical disease than conventional gadolinium (Gd) imaging (r, 0.83 for nanoparticles vs. 0.71 for Gd-imaging, $P < 0.001$). We validated our approach using the Food and Drug Administration-approved iron oxide nanoparticle ferumoxytol. Our results show that noninvasive molecular imaging of innate immune responses can serve as an imaging biomarker of disease activity in autoimmune-mediated neuroinflammation with potential clinical applications in a wide range of inflammatory diseases.

MRI | nanoparticle imaging | USPIO | multiple sclerosis | EAE

Multiple sclerosis (MS) is a devastating neurological condition that exhibits predominant white matter (WM) but also gray matter (GM) injury (1). Its animal model, experimental autoimmune encephalomyelitis (EAE), mimics important aspects of the disease. EAE is characterized by severe demyelination and axonal degeneration caused by infiltrating T cells, B cells, and innate immune cells (2). It is well established that innate immune cells, including tissue-resident microglia and recruited macrophages, are potent mediators of tissue damage (3). Blocking their activity or skewing macrophages toward an anti-inflammatory subtype ameliorates EAE and MS. Clinical diagnosis and treatment monitoring are performed mainly by MRI (4). So far, MRI markers of the disease are based on indirect parameters such as edema, gliosis, and the disruption of the

blood–brain barrier (BBB) [as assessed by gadolinium (Gd) contrast agents]. Recently, additional contrast agents have become available that are based on magnetic nanoparticles with phagocyte tropism to target inflammatory effector cells directly (5). These nanoparticles (ultra small paramagnetic iron oxide nanoparticles, USPIOs) are phagocytosed by activated tissue-resident phagocytes and circulating myeloid effector cells that migrate to inflammatory sites. Thus, magnetic nanoparticle-enhanced MRI allows cell tracking and an estimation of the inflammatory burden. Direct imaging of effector cells that mediate inflammation and tissue damage would be desirable but has not been introduced into clinical practice despite several preclinical and clinical feasibility studies (6–12). For the detection of active MS lesions, Gd-enhanced imaging remains the gold standard but has limited

Significance

Multiple sclerosis is a devastating neurological condition that can affect the entire central nervous system. Innate immune cells mediate the underlying tissue damage, but visualizing these cellular culprits is currently not possible. Diagnosis and treatment monitoring are performed by MRI, but so far imaging markers are unspecific and based on secondary parameters (edema/gliosis; blood–brain barrier disruption). We used a nanoparticle-based approach to image brain-resident and infiltrating innate immune cells in inflammatory lesions. Nanoparticle uptake is specific for innate immune cells and correlates with clinical severity. Thus, targeting innate immunity by molecular imaging may serve as a direct marker of disease activity with the potential of clinical translation to a wide variety of inflammatory conditions for improved diagnosis and treatment monitoring.

NEUROSCIENCE

sensitivity and specificity. Here, USPIOs might add diagnostic value (6). Gd visualizes only BBB disruption (BBB-D), a non-specific effect of inflammation or other pathological states. One unresolved controversy relates to the cell types targeted by magnetic nanoparticles (e.g., monocytes, macrophages, or neutrophils); but assessing targeting specificity is difficult in human studies. In this preclinical study we used cross-linked iron oxide nanoparticles (CLIOs), a well-studied nanoparticle in cancer (13–15). We hypothesized that after the activation and homing of macrophages to inflammatory sites, nanoparticle-labeled immune cells could be visualized and quantified within EAE lesions. Labeling of CLIO with fluorescent dyes was used to validate MRI signals using innovative ultramicroscopy (UM) of cleared brains, confocal microscopy, and flow cytometry. Flow cytometric analyses were performed to phenotype inflammatory infiltrates. Finally, we used the Food and Drug Administration (FDA)-approved iron oxide nanoparticle ferumoxytol (16–20) to corroborate the clinical potential of our approach.

Materials and Methods

EAE Induction. Female SJL mice (6–12 wk old) were obtained from Jackson Laboratories. EAE was induced by s.c. injecting 200 μg proteolipid protein (PLP) peptide (PLP$_{139-151}$; GenScript), emulsified in 50 μL PBS and 50 μL of complete Freund's adjuvant (BD Difco, Fisher Scientific) containing 4 mg/mL heat-inactivated *Mycobacterium tuberculosis* H37 Ra (BD Difco, Fisher Scientific). Two hundred nanograms of pertussis toxin (PTx) (List Biological Laboratories) dissolved in 200 μL PBS was administered i.p. on days 0 and 2. The animal protocol was approved by the animal welfare authority (G-212-13, Regierungspräsidium Karlsruhe) and the Institutional Animal Care and Use Committee (Massachusetts General Hospital). Additional details are given in *SI Materials and Methods*.

MRI. MRI was performed on a 9.4-Tesla (T) horizontal-bore small animal MRI scanner (BioSpec 94/20 USR; Bruker BioSpin GmbH) with a four-channel phased-array receiver coil. The brain MRI protocol included a T2-weighted (T2-w) rapid acquisition with relaxation enhancement (RARE) sequence to assess edema and a T1-weighted (T1-w) fast low-angle shot (FLASH) sequence to assess BBB-D after Gd administration. A T2*-w FLASH sequence (21) was used to assess USPIO uptake. For magnetic nanoparticle imaging, we i.v. injected mice with CLIO-FITC, CLIO-TAMRA (kindly provided by R. Weissleder, Massachusetts General Hospital, Harvard Medical School, Boston), or ferumoxytol (Feraheme; AMAG Pharmaceuticals Inc.) at a concentration of 15 mg/kg diluted in 150 μL PBS. Additional details are given in *SI Materials and Methods*.

Clearing of Mouse Brains and Acquisition of UM Data. For UM analysis whole brains were optically cleared using the FluorClearBABB protocol (22, 23). Additional details are given in *SI Materials and Methods*.

Histology and Immunohistochemistry. For histological correlation analysis, mice were killed in deep anesthesia by intracardial perfusion with PBS, followed by 4% paraformaldehyde (PFA, Roti-Histofix; Carl Roth). Brains were dissected and either snap-frozen in Tissue-Tek optimum cutting temperature (O.C.T.) compound (VWR) or processed for standard paraffin histology. Five to ten-micrometer cryostat or microtome sections were cut. Stainings were performed with ionized calcium-binding adaptor molecule 1 (Iba-1) antibody (WAKO) for macrophages/microglia, with CD3 antibody (Dako) for T cells, with CD45R antibody (eBioscience) for B cells, and with myeloperoxidase (MPO) antibody (Abcam) using standard immunohistochemistry protocols. Tile scans (20× of the entire cerebellum, midbrain, and cortex) and higher-magnification images (60×) were acquired by confocal microscopy (Olympus FV1000 or Zeiss LSM700). Additional details are given in *SI Materials and Methods*.

Isolation of Immune Cells and Flow Cytometry. SJL mice were killed by an overdose of 100 mg/kg ketamine and 20 mg/kg xylazine (kx), and blood was drawn from the heart before intracardial perfusion with PBS. Brain, spinal cord, bone marrow, liver, spleen, and lymph nodes were excised. The cerebrum and cerebellum were homogenized separately. Brain leukocytes were isolated and used for flow cytometry as previously described (24). Additional details are given in *SI Materials and Methods*.

Statistical Analysis. Data are shown as mean ± SEM. Statistical analyses were performed in PRISM (GraphPad). Additional details in *SI Materials and Methods*.

Results

Cultured Macrophages Take up CLIO-FITC and Can Be Imaged by MRI. First, we examined the capacity of macrophages and microglia to phagocytose CLIO nanoparticles (Fig. 1 *A* and *B*). Monocytes from the bone marrow of healthy mice were isolated, cultivated in vitro, and polarized into M1- or M2-like macrophages using chemokine mixtures (25). We found that the two macrophage subtypes phagocytosed particles to a similar degree (Fig. 1*C*). The proportion of CLIO-labeled macrophages increased in a dose-dependent manner (Fig. 1 *D* and *E*). Importantly, in vitro-loaded macrophages exhibited a clear, dose-dependent signal drop when imaged by T2*-w MRI at 9.4 T (10^5 cells loaded with either 100 or 500 μg/mL of CLIO) (Fig. 1*F*). This result indicated that CLIO particle imaging should be feasible for in vivo studies.

PLP-Induced EAE Results in Rapidly Progressing Inflammatory Lesions. After EAE induction the first clinical symptoms developed rapidly, 6–12 d after immunization (Fig. 2 *A* and *B*). At disease onset (baseline MRI) animals were imaged by high-field 9.4-T MRI using T2-w, T2*-w, and T1-w post-Gd contrast sequences (Fig. 2*C*). Strong, confluent Gd enhancement and concomitant edema were present in the cerebellar WM and around the meninges. Gd enhancement, however, represents only BBB-D rather than actual inflammation. Hence, more direct means to assess inflammation by MRI would be desirable (26). To determine whether more specific imaging of inflammation and cell tracking was possible in our model, we i.v. injected CLIO-FITC. CLIO injection led to an immediate loss of vascular signal and the delineation of the vasculature (Fig. S1*A*). Forty-eight hours after CLIO administration, free particles were largely cleared from the circulation and had accumulated in immune cells of spleen, liver, lymph nodes, blood, and bone marrow, as assessed by MRI and flow cytometry (Fig. S1). This time point (onset + 2) was used for follow-up MRI to assess cellular influx. T2*-w imaging before contrast administration (pre CLIO) outlines venules because of the blood oxygenation level-dependent (BOLD) contrast of deoxygenized blood (Fig. 2*C*). Forty-eight hours after CLIO administration (post CLIO) additional linear and punctate susceptibility signals were found (Fig. 2*D*). CLIO deposition in the cerebellum localized mainly to the WM, and image subtraction (post CLIO minus pre CLIO) facilitated its identification (Fig. 2*E*).
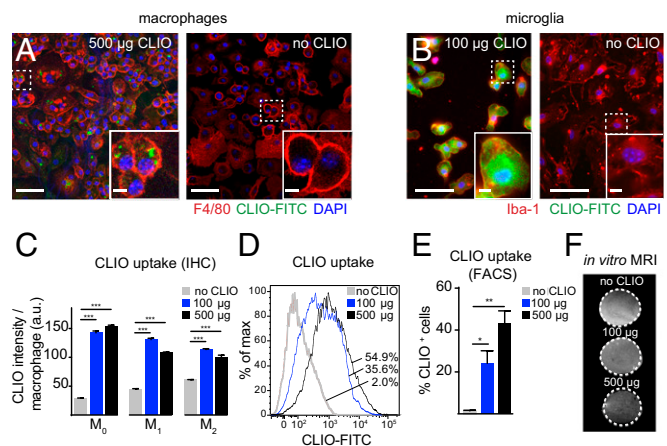

Fig. 1. Cultured macrophages and microglia phagocytose CLIO-FITC. (*A* and *B*) Confocal images of bone marrow-derived macrophages (BMDMs) (*A*) and microglia (*B*) incubated with or without CLIO-FITC (500 μg/mL and 100 μg/mL, respectively). (*C*) Quantification of immunohistochemistry of CLIO uptake per macrophage subtype. (*D*) Representative flow cytometry histogram of CLIO uptake by macrophages. Numbers indicate the respective frequency of CLIO$^+$ cells. (*E*) Quantification of flow cytometry data. (*F*) T2*-w MRI of macrophages incubated with CLIO-FITC. BMDMs (10^5) were incubated for 2 h with or without CLIO. *n* = 3 independent biological replicates for *C*–*F*. (Scale bars: 50 μm for overview images in *A* and *B*; 5 μm for magnified *Insets*.)

Because T2* imaging is prone to image artifacts caused by magnetic field inhomogeneity and motion of the animal (e.g., breathing), T2* imaging of CLIO-injected animals was performed in a subset of animals ex vivo after brain explantation to confirm iron particle deposition. Strong susceptibility signals were found in the cerebellum, basal ganglia, and cortex. Such signals were found only in diseased animals; healthy animals did not show nanoparticle uptake (Fig. 2F).

Nanoparticle Uptake Correlates with Clinical Disease Severity. Quantification of T2* images revealed a 4.6-fold increase in cerebellar susceptibility signals 48 h after CLIO injection in diseased animals (cerebellar volume of T2* signal drop before injection: 1.33 ± 0.50 mm^3, vs. 6.14 ± 0.82 mm^3 after CLIO injection, $P < 0.001$) (Fig. 2G). Importantly, the volume of the decrease in T2* signal in the cerebellum correlated better with disease severity (Spearman's r: 0.83, $P < 0.001$) than did conventional Gd enhancement (Spearman's r: 0.71, $P < 0.01$) (Fig. 2 H and I).

Nanoparticles Localize to Infiltrating Macrophages and Resident Microglia in Vivo. To validate that iron oxide nanoparticles indeed accumulate in inflammatory phagocytic cells, we performed immunohistochemical stainings for Iba-1, a marker for macrophages and microglia (27). Dense infiltrates of Iba-1$^+$ macrophages and microglia were present throughout the cerebellar WM and had largely phagocytosed nanoparticles (Fig. 3A). Immunohistochemical quantifications showed that most macrophages/microglia infiltrates localize to the WM (7.0×10^2 Iba-1$^+$ cells/mm^2 in the WM compared with 4.6×10^2/mm^2 in the GM and 1.6×10^2/mm^2 in the cerebellar WM of healthy controls, $P < 0.05$) (Fig. 3B). Most macrophages/microglia had accumulated CLIO-FITC ($P < 0.05$) (Fig. 3C). B cells and T cells did not show CLIO-FITC uptake (Fig. 3 D and E). In some animals Gd-enhanced MRI also showed prominent lesions in the midbrain (24%, $n = 8$ mice from 33 animals total, four independent experiments) and cortex (30%, $n = 10$ mice), with concomitant iron oxide deposition (Fig. 3 F and G). Immunohistochemistry showed infiltrates of macrophages/microglia with particle uptake (Fig. 3 H and I). The levels of uptake in the cortex were considerably smaller than in the cerebellum ($3.7 \pm 0.6 \times 10^2$ Iba-1$^+$/CLIO$^+$ cells/mm^2 in the cerebellum vs. $1.1 \pm 0.2 \times 10^2$ cells/mm^2 in the cortex; $P < 0.05$). To better understand how CLIO labels microglia, we killed EAE animals 2 h after CLIO administration after having proven BBB-D by Gd-enhanced MRI (Fig. S2A). CLIO was present both around blood vessels and in the parenchyma within inflammatory lesions close to Iba-1$^+$ cells (Fig. S2 B and C). However, macrophages/microglia were CLIO$^-$ at this early time point (Fig. S2B), indicating that they phagocytose free particles over time. CD31$^+$ vessels did not show CLIO uptake when assessed 48 h after CLIO injection (Fig. S2D). Next, we assessed axonal pathology and demyelination, both hallmarks of EAE and MS. We found large demyelinated areas in the cerebellar WM in Luxol Fast Blue stainings. Corresponding regions showed severe axonal damage with disrupted tissue morphology on neurofilament protein (NFP) stainings (Fig. S2 E and F). Inflammatory changes as assessed by immunohistochemistry for the inflammatory enzyme MPO were present in the WM and GM matter of the cerebellum (Fig. 3J). To assess the 3D distribution of the nanoparticles further, we performed tissue clearing with FluorClearBABB (23). Clearing of EAE brains and UM confirmed widespread lesions in the cerebellar WM, cortex, and midbrain (Fig. 3K and Movie S1). In contrast, there were no MRI signal changes, CLIO particle uptake, or MPO expression in healthy control animals (Fig. 3K and Fig. S3).

Nanoparticle Uptake Occurs Predominantly in the Acute Phase of the Disease. To determine the degree of macrophage influx during the remission phase of EAE, we performed a time-course experiment. After the administration of CLIO-FITC at the onset of disease, we reinjected the same animal with CLIO-TAMRA in the remission phase (10–14 d after symptom onset), followed by MRI and histological assessment (Fig. 2A). On immunohistochemical analysis we found predominantly CLIO-FITC that was widespread within the cerebellum but only traces of
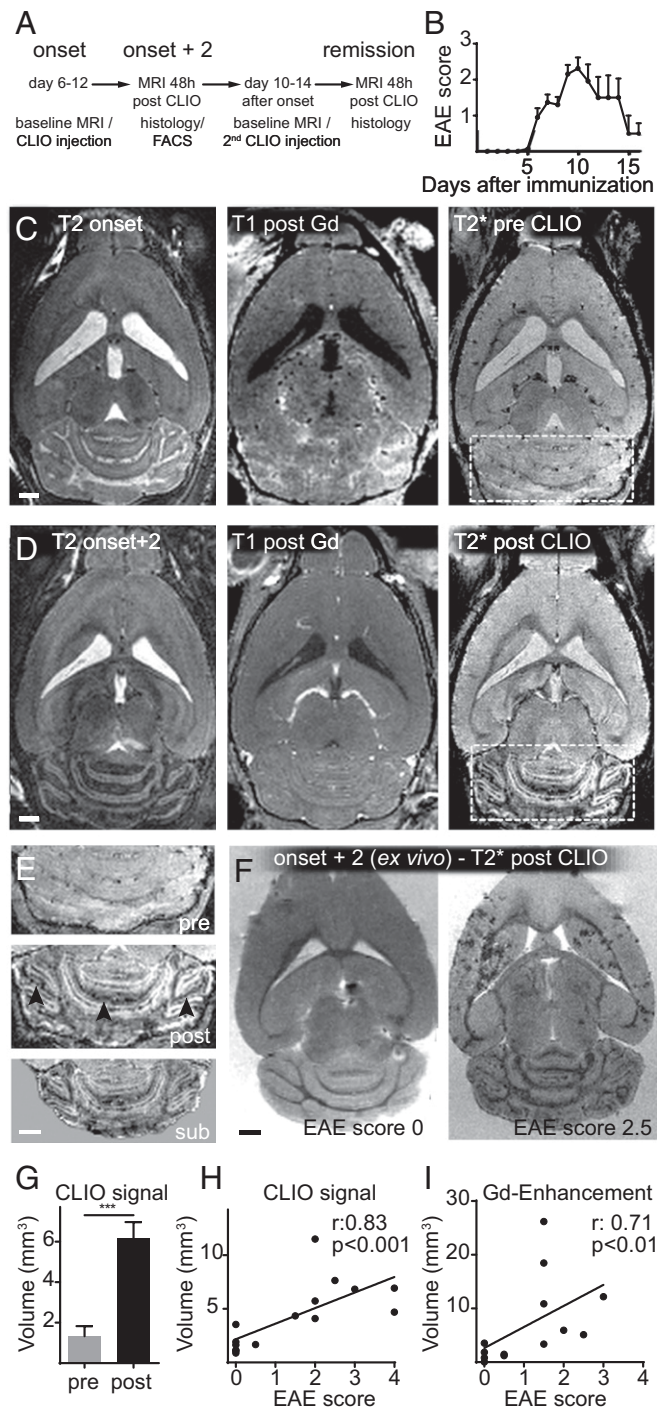

Fig. 2. In vivo nanoparticle uptake can be quantified by MRI. (A) Experimental outline. (B) EAE scores. (C and D) T2-w, T1-w after Gd, and T2*-w MRI before CLIO at onset of disease (C) and 2 d after disease onset (48 h after CLIO injection) (D). (E) Magnification of the cerebellum before (pre) (Top) and 48 h after CLIO administration (post) (Middle). (Bottom) The subtraction image (post CLIO minus pre CLIO). (F) Ex vivo T2* images 48 h after CLIO administration of a healthy (clinical score 0) and severely affected EAE animal (score 2.5. (G) Cerebellar volume with signal decrease on T2*-w images. (H) Correlation analysis of the volume of T2* signal decrease and the clinical score. (I) Correlation analysis of the volume of Gd enhancement and the clinical score. (Scale bars: 1 mm.)
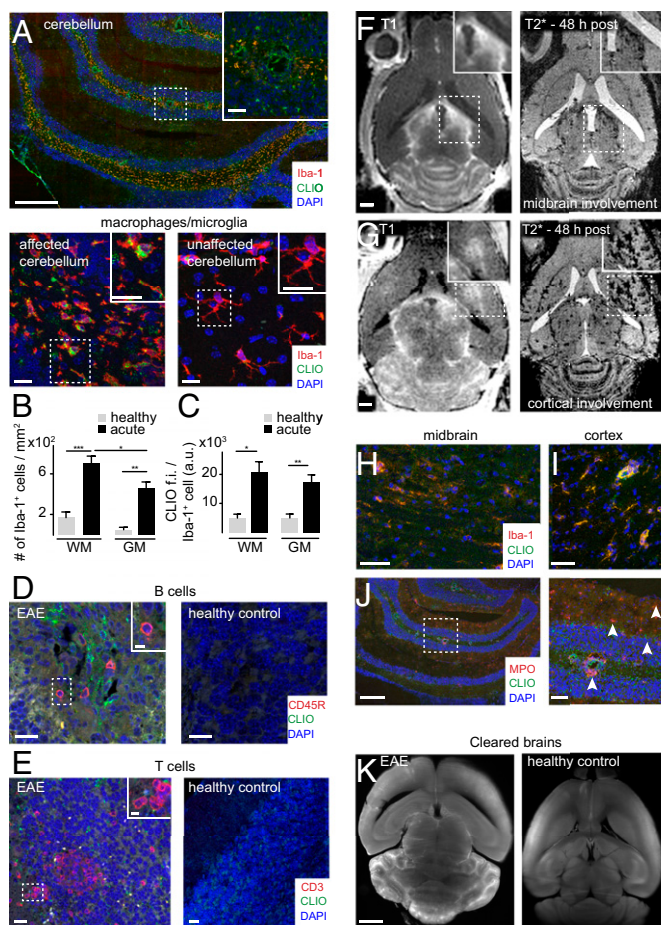
Fig. 3. Immunohistochemistry of immune cell infiltrates. (*A*) Confocal image (tile scan) of Iba-1$^+$ macrophages/microglia in the cerebellum. CLIO-FITC was administered 48 h before. (*B* and *C*) Quantification of Iba-1$^+$ cells (*B*) and CLIO-FITC uptake (*C*) in the cerebellar GM and WM ($n = 7$ mice for the acute EAE group and $n = 3$ mice for the healthy control group). a.u., arbitrary units; f.i., fluorescence intensity. (*D* and *E*) Confocal images of B cells (CD45R) (*D*) and T cells (CD3) (*E*) in EAE and healthy controls. (*F–I*) MRI (*F* and *G*) and immuno-histochemistry (*H* and *I*) of cortical and midbrain lesions. (*J*) Staining for the in-flammatory enzyme MPO. Arrowheads indicate MPO$^+$ cells. (*K*) Representative section of a FluorClearBABB-cleared EAE brain and a healthy control brain 48 h after CLIO injection, acquired by UM. Brain clearing was performed in three EAE mice and three CLIO-injected healthy controls. (Magnification: *K*, 1×.) Confocal images were recorded as tile scans (composite image). (Scale bars: 500 μm for the overview image in *A*, *Upper*; 100 μm for the *Inset* in the overview in *A*; 20 μm for the magnified images in *A*, *Lower*; 20 μm for overview images in *D* and *E*; 5 μm for *Insets* In *D* and *E*; 1 mm in *F*, *G*, and *K*; 50 μm in *H* and *I*; 500 μm for the overview image in *J*; 100 μm for the magnified image in *J*.)

CLIO-TAMRA. Macrophages/microglia were present only around major vessels, and most focal cerebellar lesions had resolved (Fig. S4*A*). Also, when we quantified Iba-1$^+$cells, we only found a minor increase in macrophages/microglia compared with healthy control animals (a 3.3-fold increase of Iba-1$^+$ cells in the cerebellar WM, $P < 0.01$, $n = 3$ mice). Iba-1$^+$ cell numbers and CLIO uptake in the cerebellar GM were not statistically different in remission-phase animals and healthy control animals, indicating that inflammation had mostly resolved ($P > 0.05$) (Fig. S4 *B* and *C*).

The Majority of Myeloid Effector Cells Phagocytose Nanoparticles. To better understand the cellular contribution to the MRI signal at the single cell level, we performed flow cytometry analysis. Cerebellum and cerebrum were assessed separately because the cerebellum is more severely affected by the disease than the cerebrum. EAE brains were isolated into single cells and stained for CD45,

CD11b, and Ly6G to differentiate infiltrating macrophages (CD11b$^+$, CD45^{high}, Ly-6G$^-$), resident microglia (CD11b$^+$, CD45$^{intermediate/low}$), and neutrophils (Ly-6G$^+$, CD45$^+$). We further stained T cells (CD45^{high}, CD11b$^-$, CD3$^+$, CD4$^+$, or CD8$^+$) and B cells (CD45^{high}, CD11b$^-$, B220$^+$) (Fig. 4 *A* and *B* and Fig. S5 *A* and *B*). As expected there was a marked increase of macrophages, microglia, and neutrophils in EAE (11.9 ± 2.7% of macrophages compared with <1% in the healthy brain, $P < 0.05$; 21.0 ± 4.2% of microglia vs. 6.4 ± 1.6%, $P = 0.05$) (Fig. 4 *C–G*). A large proportion of these inflammatory myeloid effector cells took up CLIO (49.0 ± 7.1% of cerebellar macrophages in EAE vs. 9.9 ± 2.8% in the healthy control, $P < 0.01$) (Fig. 4 *C*, *F*, and *G*). To pinpoint further the extent to which different macrophage sub-types contribute to nanoparticle uptake, we stained for Ly-6C, a marker of macrophage activation (28). In line with our ex vivo polarization experiments, Ly-6C^{high} and Ly-6C^{low} monocytes/macrophages did not differ significantly in their degree of nano-particle uptake, although there was a trend toward more uptake by the Ly-6C^{high} subpopulation ($P > 0.05$) (Fig. S5*C*). The strong nano-particle uptake of myeloid effector cells was in contrast to T cells and B cells, which took up significantly less CLIO (11.4 ± 3.5%, $P = 0.01$ compared with macrophages), and the innate immune cell compart-ment encompassed >85% of all CLIO$^+$ leukocytes (Fig. S5*D*). Similar results were obtained in the cerebrum, with largely innate immune cell labeling and only sparse labeling of adaptive immune cells (Fig. 4 *E* and *G*) and spinal cord (Fig. S5*E*). Interestingly, both the macrophage number and the degree of CLIO uptake correlated with the clinical score of the individual animal (Spearman's r: 0.72, $P < 0.001$, and 0.76, $P < 0.001$, respectively) (Fig. 4 *H* and *I*).

MR Imaging with the FDA-Approved Compound Ferumoxytol Confirms Clinical Applicability. To validate the clinical potential of our ap-proach, we used the FDA-approved iron oxide nanoparticle fer-umoxytol to image inflammatory lesions in acute EAE. Using the same approach as with the experimental CLIO particle, we found a precise delineation of hypointense ferumoxytol signal, mainly in the cerebellar WM (Fig. 5 *A–C*). Quantification of the ferumoxytol signal showed a 5.8-fold increase in hypointense signal 24 h after ferumoxytol administration (volume of signal decrease for fer-umoxytol: 5.8 ± 0.7 mm^3 vs. 1.0 ± 0.3 mm^3 before ferumoxytol, $P = 0.01$) (Fig. 5*D*). Iron staining confirmed iron-positive cells (most likely macrophages/microglia) in the cerebellar WM in ferumoxytol-injected animals which were not detectable in healthy control animals (Fig. 5*E*).

Discussion

Diagnosis and monitoring of disease activity in MS is mainly based on Gd-enhanced MRI (29, 30), which assesses the integrity of the BBB. However, Gd imaging has limited sensitivity and specificity and does not reflect the activity of cellular disease mediators (30). Moreover, its correlation to important clinical parameters (like the Expanded Disability Status Scale) and to pathological hallmarks such as de-myelination and neurodegeneration is limited (30). Direct imaging of molecular targets or cellular effector cells of tissue damage would be highly desirable (8, 26, 31, 32). We have established a protocol to image myeloid effector cells and BBB-D sequentially using innovative magnetic nanoparticles followed by Gd-imaging. Our results illustrate that the T2* signal attenuation specifically shows different innate immune cells (macrophages, activated microglia, and neutrophils). Furthermore, MRI signal quantification of phagocytic activity cor-relates with disease severity. This correlation was confirmed on the cellular level where CLIO uptake by macrophages correlated signif-icantly with the clinical score. Iron oxide nanoparticle imaging has been performed in a wide variety of diseases (16, 17, 33–35), but apart from liver imaging (36), iron oxide imaging has not yet been translated into clinical practice, partially because of economic, safety, and technical reasons (37–40). However, imaging of inflammation is of major clinical interest. Areas of unmet need that would require imaging of inflammation and immune cell responses include immunotherapy of cancer and autoimmune conditions such as
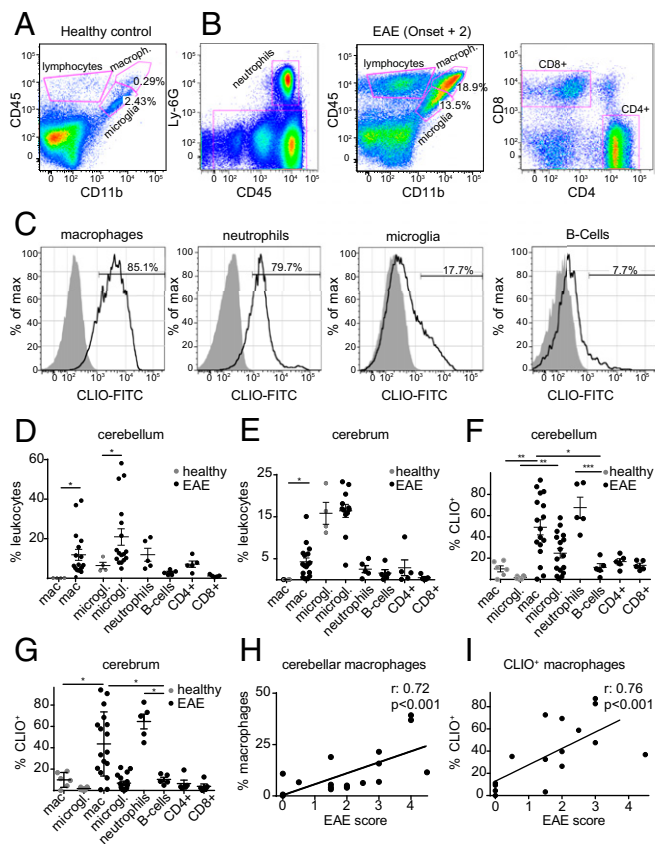
Fig. 4. CLIO uptake of innate immune cells correlates with clinical severity. (*A* and *B*) Representative FACS plots for healthy control (*A*) and EAE (*B*) animals at onset + 2. Gating strategies are shown for the identification of the respective leukocyte subsets. (*C*) Histogram of CLIO⁺ cells for each cell population. (*D* and *E*) Flow cytometry quantification in the cerebellum (*D*) and cerebrum (*E*). (*F* and *G*) Percentage of CLIO⁺ cells. (*H*) Spearman correlation analysis of cerebellar macrophage frequency and EAE score. (*I*) Correlation analysis of CLIO⁺ cerebellar macrophage frequency and EAE score. Dots in *D–I* indicate single animals. $n = 4$ mice for healthy controls and $n = 5–19$ mice for EAE groups. Flow cytometry data are pooled from three independent experiments.

MS. For these applications, iron oxide nanoparticles could allow patient stratification and treatment monitoring (19, 33, 41).

The current study extends previous work on USPIOs that were used mainly in cardiovascular disease, in tumor models, and in small clinical trials (13, 16, 17). In the present study we first confirmed the efficient labeling of macrophages and microglia in vitro. We further validated that macrophages, microglia, and neutrophils take up USPIOs in vivo and quantified the uptake for each cell type. Despite evidence that neutrophils may promote autoimmune neuroinflammation (42), the high frequency of Ly-6G⁺ cells may signify that this population also contains eosinophils, differentiating premonocytes, or plasmacytoid dendritic cells, all of which have been reported to express Ly6-G under certain conditions, and might be present in EAE lesions. Nanoparticle uptake by adaptive immune cells was only marginal, indicating that nanoparticle imaging is predominantly a marker of innate immunity. We found that in healthy animals innate CD11b⁺ cells take up CLIO by a much higher frequency than T cells and B cells and also phagocytose more particles per cell. We calculated that 86–94% of the signal originates from myeloid cells, depending on the respective organ (e.g., spleen vs. blood). In EAE we identified CLIO labeling of T cells and B cells by flow cytometry (up to 20% of T cells). Again, myeloid cells take up more CLIO per cell based on median fluorescence intensity in flow cytometry. In immunohistochemistry we did not detect CLIO uptake by B cells or T cells. Taking these

findings together, we estimate that more than 90% of the nanoparticle signal in EAE originates from innate immune cells (Fig. S5*D*). The degree of adaptive immune cell labeling, which would partially diminish the specificity of the imaging approach, is most likely the result of the uptake mechanism. It has been proposed that macropinocytosis is the entry mechanism of iron oxide nanoparticles, a mechanism that most cell types are capable of using, although to a very different degree (5). Thus, we concluded that our imaging approach in EAE shows innate immune responses, but signal origin in other disease models will depend on the cellular micromilieu of the respective pathology.

We also illustrate different lesion types (cerebellar WM and GM, midbrain, and cortical lesions) that evolve in this MS model. Severe inflammation was also present in the spinal cord. In contrast to myelin oligodendrocyte glycoprotein (MOG) EAE in C57BL/6 mice, which exhibits mainly spinal pathology, PLP immunization in SJL mice leads to widespread cerebral pathology (31, 32). We found prominent immune cell infiltrates mostly in the cerebellum but also in the midbrain and cortex. This localization seems especially relevant because GM and cortical pathology is of major clinical relevance (1, 43, 44), and so far insights into the underlying mechanisms of neurodegeneration are limited (45, 46). One limitation of many studies that use experimental contrast agents relates to the clinical translatability of the work. We used experimental CLIO particles that are not available for clinical use but are well characterized in experimental models, are fluorescently labeled, and showed good uptake and biodistribution kinetics. To show the clinical potential, we also performed experiments with the FDA-approved agent ferumoxytol that has been used "off label" for human imaging studies (18, 19). Using this agent, we validated our approach and demonstrated that ferumoxytol imaging could be a valid strategy for nanoparticle imaging in the clinical arena, although safety issues with the agent might apply (37). In our study we used a high-field preclinical MRI system (9.4 T) that has better sensitivity than 3T scanners for the detection of susceptibility signals caused by iron oxide nanoparticles. Nevertheless, several studies have demonstrated that USPIO imaging is feasible in the clinical setting (17–19). Another limitation is the imaging target itself. Although macrophages and microglia are important effector cells in EAE and MS (3), our imaging approach does not reflect the entire cellular complexity of the disease. B cells and T cells are additional imaging targets that are more difficult to label by iron oxide nanoparticles (13, 47). Another aspect is a possible interaction of the particle with immune cell functions. Previous studies have investigated the capacity of different human
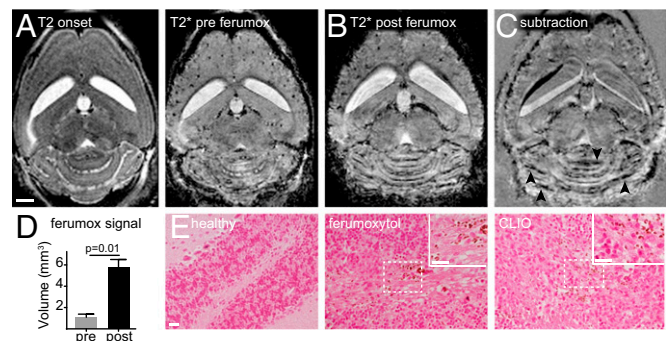

Fig. 5. Ferumoxytol imaging delineates EAE lesions. (*A* and *B*) T2-w and T2*-w images at disease onset before ferumoxytol injection (*A*) and 1 d after EAE onset (24 h post ferumoxytol injection) (*B*). (*C*) Subtraction image (post ferumoxytol minus pre ferumoxytol) demonstrates signal loss in areas of ferumoxytol deposition (arrowheads). (*D*) Cerebellar volume with signal decrease on T2*-w images pre and post ferumoxytol administration. (*E*) Micrographs of DAB-enhanced Prussian blue staining for iron. CLIO section is shown as a positive control. $n = 4$ mice. (Scale bars: 1 mm in *A–C*; 20 μm in *E*.)

immune cell populations to phagocytose USPIOs and the possible effects of particle labeling on immune cell function (48). We did not observe differences in disease severity or onset in USPIO-injected vs. noninjected animals, indicating that USPIO labeling did not greatly interfere with immune cell function; however, we did not investigate this issue in depth.

In summary, we demonstrate high sensitivity and cellular specificity for innate immune cells using USPIO imaging in an MS model and noninvasively track infiltrating neutrophils, macrophages, and activated microglia by longitudinal MRI. USPIO imaging provides a tool for innate immune cell tracking that, in contrast to conventional Gd imaging, reflects cellular disease mechanisms. Thus, it can serve as an imaging biomarker for inflammatory disease severity and directly show the underlying cellular culprits of disease. This study could spur research to translate iron oxide nanoparticle imaging into clinical practice for patients suffering from MS and other innate immunity-driven diseases.

1. Trapp BD, Nave K-A (2008) Multiple sclerosis: An immune or neurodegenerative disorder? *Annu Rev Neurosci* 31(1):247–269.
2. Wekerle H, Flügel A, Fugger L, Schett G, Serreze D (2012) Autoimmunity's next top models. *Nat Med* 18(1):66–70.
3. Hemmer B, Kerschensteiner M, Korn T (2015) Role of the innate and adaptive immune responses in the course of multiple sclerosis. *Lancet Neurol* 14(4):406–419.
4. Wattjes MP, et al.; MAGNIMS study group (2015) Evidence-based guidelines: MAGNIMS consensus guidelines on the use of MRI in multiple sclerosis–establishing Disease prognosis and monitoring patients. *Nat Rev Neurol* 11(10):597–606.
5. Weissleder R, Nahrendorf M, Pittet MJ (2014) Imaging macrophages with nanoparticles. *Nat Mater* 13(2):125–138.
6. Tourdias T, et al. (2012) Assessment of disease activity in multiple sclerosis phenotypes with combined gadolinium- and superparamagnetic iron oxide-enhanced MR imaging. *Radiology* 264(1):225–233.
7. Millward JM, et al. (2013) Iron oxide magnetic nanoparticles highlight early involvement of the choroid plexus in central nervous system inflammation. *ASN Neuro* 5(1):e00110.
8. Dousset V, et al. (2006) MR imaging of relapsing multiple sclerosis patients using ultra-small-particle iron oxide and compared with gadolinium. *AJNR Am J Neuroradiol* 27(5):1000–1005.
9. Linker RA, et al. (2006) Iron particle-enhanced visualization of inflammatory central nervous system lesions by high resolution: Preliminary data in an animal model. *AJNR Am J Neuroradiol* 27(6):1225–1229.
10. Ladewig G, et al. (2009) Spatial diversity of blood-brain barrier alteration and macrophage invasion in experimental autoimmune encephalomyelitis: A comparative MRI study. *Exp Neurol* 220(1):207–211.
11. Dousset V, et al. (1999) Comparison of ultrasmall particles of iron oxide (USPIO)-enhanced T2-weighted, conventional T2-weighted, and gadolinium-enhanced T1-weighted MR images in rats with experimental autoimmune encephalomyelitis. *AJNR Am J Neuroradiol* 20(2):223–227.
12. Kleinschnitz C, et al. (2003) In vivo monitoring of macrophage infiltration in experimental ischemic brain lesions by magnetic resonance imaging. *J Cereb Blood Flow Metab* 23(11):1356–1361.
13. Kircher MF, et al. (2003) In vivo high resolution three-dimensional imaging of antigen-specific cytotoxic T-lymphocyte trafficking to tumors. *Cancer Res* 63(20):6838–6846.
14. Leimgruber A, et al. (2009) Behavior of endogenous tumor-associated macrophages assessed in vivo using a functionalized nanoparticle. *Neoplasia* 11(5):459–468.
15. Kircher MF, Mahmood U, King RS, Weissleder R, Josephson L (2003) A multimodal nanoparticle for preoperative magnetic resonance imaging and intraoperative optical brain tumor delineation. *Cancer Res* 63(23):8122–8125.
16. Daldrup-Link HE, et al. (2011) MRI of tumor-associated macrophages with clinically applicable iron oxide nanoparticles. *Clin Cancer Res* 17(17):5695–5704.
17. Dósa E, et al. (2011) Magnetic resonance imaging of intracranial tumors: Intra-patient comparison of gadoteridol and ferumoxytol. *Neuro-oncol* 13(2):251–260.
18. Rashidian M, et al. (2015) Noninvasive imaging of immune responses. *Proc Natl Acad Sci USA* 112(19):6146–6151.
19. Gaglia JL, et al. (2015) Noninvasive mapping of pancreatic inflammation in recent-onset type-1 diabetes patients. *Proc Natl Acad Sci USA* 112(7):2139–2144.
20. McConnell HL, et al. (2016) Ferumoxytol nanoparticle uptake in brain during acute neuroinflammation is cell-specific. *Nanomedicine (Lond)* 12(6):1535–1542.
21. Park S-H, Masamoto K, Hendrich K, Kanno I, Kim S-G (2008) Imaging brain vasculature with BOLD microscopy: MR detection limits determined by in vivo two-photon microscopy. *Magn Reson Med* 59(4):855–865.
22. Breckwoldt MO, et al. (2016) Correlated magnetic resonance imaging and ultramicroscopy (MR-UM) is a tool kit to assess the dynamics of glioma angiogenesis. *eLife* 5:e11712.
23. Schwarz MK, et al. (2015) Fluorescent-protein stabilization and high-resolution imaging of cleared, intact mouse brains. *PLoS One* 10(5):e0124650.
24. Pulli B, et al. (2015) Multiple sclerosis: Myeloperoxidase immunoradiology improves detection of acute and chronic disease in experimental model. *Radiology* 275(2):480–489.
25. Ying W, Cheruku PS, Bazer FW, Safe SH, Zhou B (2013) Investigation of macrophage polarization using bone marrow derived macrophages. *J Vis Exp* June 2013(76):50323.
26. Vellinga MM, et al. (2008) Pluriformity of inflammation in multiple sclerosis shown by ultra-small iron oxide particle enhancement. *Brain* 131(Pt 3):800–807.
27. Mildner A, et al. (2007) Microglia in the adult brain arise from Ly-6ChiCCR2+ monocytes only under defined host conditions. *Nat Neurosci* 10(12):1544–1553.
28. Swirski FK, et al. (2007) Ly-6Chi monocytes dominate hypercholesterolemia-associated monocytosis and give rise to macrophages in atheromata. *J Clin Invest* 117(1):195–205.
29. Montalban X, et al. (2010) MRI criteria for MS in patients with clinically isolated syndromes. *Neurology* 74(5):427–434.
30. Daumer M, Neuhaus A, Morrissey S, Hintzen R, Ebers GC (2009) MRI as an outcome in multiple sclerosis clinical trials. *Neurology* 72(8):705–711.
31. Chen JW, Breckwoldt MO, Aikawa E, Chiang G, Weissleder R (2008) Myeloperoxidase-targeted imaging of active inflammatory lesions in murine experimental autoimmune encephalomyelitis. *Brain* 131(Pt 4):1123–1133.
32. Forghani R, et al. (2012) Demyelinating diseases: Myeloperoxidase as an imaging biomarker and therapeutic target. *Radiology* 263(2):451–460.
33. Harisinghani MG, et al. (2003) Noninvasive detection of clinically occult lymph-node metastases in prostate cancer. *N Engl J Med* 348(25):2491–2499.
34. Lewin M, et al. (2000) Tat peptide-derivatized magnetic nanoparticles allow in vivo tracking and recovery of progenitor cells. *Nat Biotechnol* 18(4):410–414.
35. Kleinschnitz C, et al. (2003) In vivo monitoring of macrophage infiltration in experimental ischemic brain lesions by magnetic resonance imaging. *J Cereb Blood Flow Metab* 23(11):1356–1361.
36. Tanimoto A, Kuribayashi S (2006) Application of superparamagnetic iron oxide to imaging of hepatocellular carcinoma. *Eur J Radiol* 58(2):200–216.
37. Muehe AM, et al. (2016) Safety Report of Ferumoxytol for Magnetic Resonance Imaging in Children and Young Adults. *Invest Radiol* 51(4):221–227.
38. Kiessling F, Mertens ME, Grimm J, Lammers T (2014) Nanoparticles for imaging: Top or flop? *Radiology* 273(1):10–28.
39. Corot C, Warlin D (2013) Superparamagnetic iron oxide nanoparticles for MRI: Contrast media pharmaceutical company R&D perspective. *Wiley Interdiscip Rev Nanomed Nanobiotechnol* 5(5):411–422.
40. Harms C, et al. (2013) Certain types of iron oxide nanoparticles are not suited to passively target inflammatory cells that infiltrate the brain in response to stroke. *J Cereb Blood Flow Metab* 33(5):e1–e9.
41. Okada H, et al. (2015) Immunotherapy response assessment in neuro-oncology: A report of the RANO working group. *Lancet Oncol* 16(15):e534–e542.
42. Lévesque SA, et al. (2016) Myeloid cell transmigration across the CNS vasculature triggers IL-1β-driven neuroinflammation during autoimmune encephalomyelitis in mice. *J Exp Med* 213(6):929–949.
43. Daams M, Geurts JJG, Barkhof F (2013) Cortical imaging in multiple sclerosis: Recent findings and 'grand challenges'. *Curr Opin Neurol* 26(4):345–352.
44. Fischer MT, et al. (2013) Disease-specific molecular events in cortical multiple sclerosis lesions. *Brain* 136(Pt 6):1799–1815.
45. Nikić I, et al. (2011) A reversible form of axon damage in experimental autoimmune encephalomyelitis and multiple sclerosis. *Nat Med* 17(4):495–499.
46. Jürgens T, et al. (2016) Reconstruction of single cortical projection neurons reveals primary spine loss in multiple sclerosis. *Brain* 139(Pt 1):39–46.
47. Pittet MJ, Swirski FK, Reynolds F, Josephson L, Weissleder R (2006) Labeling of immune cells for in vivo imaging using magnetofluorescent nanoparticles. *Nat Protoc* 1(1):73–79.
48. Settles M, et al. (2011) Different capacity of monocyte subsets to phagocytose iron-oxide nanoparticles. *PLoS One* 6(10):e25197.
49. Saura J, Tusell JM, Serratosa J (2003) High-yield isolation of murine microglia by mild trypsinization. *Glia* 44(3):183–189.